Geophys. J. Int. (1995) **120,** 677–692

Low-frequency elastic-wave scattering by an inclusion: limits of applications

Roland Gritto, Valeri A. Korneev and Lane R. Johnson

Department of Geology and Geophysics, and Center for Computational Seismology, Earth Science Division, Lawrence Berkeley Laboratory, University of California, Berkeley, CA 94720, *USA*

Accepted 1994 August 14. Received 1994 July 14; in original form 1994 March 12

SUMMARY

The present investigation considers various approximations for the problem of low-frequency elastic waves scattered by a single, small inclusion of constant elastic parameters. For the Rayleigh approximation containing both near- and far-field terms, the scattered amplitudes are investigated as a function of distance from the scatterer. Near-field terms are found to be dominant for distances up to two wavelengths, after which far-field solutions correctly describe the scattered field. At a distance of two wavelengths the relative error between the total and the far-field solution is about 15 per cent and decreases with increasing distance. Deriving solutions for the linear and quadratic Rayleigh–Born approximation, the relative error between the non-linear Rayleigh approximation and the linear and quadratic Rayleigh–Born approximation as a function of the scattering angle and the parameter perturbation is investigated. The relative error reveals a strong dependence on the scattering angle, while the addition of the quadratic term significantly improves the approximation for all scattering angles and parameter perturbations. An approximation for the error caused by linearization of the problem, based entirely on the perturbations of the parameters from the background medium, and its validity range are given. We also investigate the limit of the wave parameter for Rayleigh scattering and find higher values than previously assumed. By choosing relative errors of 5 per cent, 10 per cent and 20 per cent between the exact solution and the Rayleigh approximation, we find the upper limits for the parameter k_pR to be 0.55, 0.7 and 9.9, respectively.

Key words: elastic waves, Rayleigh–Born approximation, Rayleigh limit, Rayleigh scattering.

1 INTRODUCTION

Scattering of seismic waves is a fundamental process in the propagation of waves through the Earth. In recent years, numerous authors have turned to the theory of scattering to describe the complicated nature of seismograms that occur in various places, believed to be caused by inhomogeneities and sequences of layering within the structure of the Earth. Different scale lengths are the focus of attention, varying from mantle (Haddon & Cleary 1974; Doornbos 1976; Aki 1980), over crustal (Aki 1969; Wu 1982; Sato 1984), to regional and even local scales on the order of a few metres (Wu & Aki 1985; Herraiz & Espinosa 1987; Sams & Goldberg 1990). The common objective of these studies is to apply statistical approaches to determine the heterogeneity and the elastic parameters of the medium and to distinguish between different attenuation processes like intrinsic and scattering attenuation (Frankel & Clayton 1986; Frankel & Wennerberg 1987; Frankel 1991). Lately, the theory of localization, well established in quantum mechanics, solid-state physics and optics, was introduced to seismology (O'Doherty & Anstey 1971) to investigate scattering processes during propagation, and to determine possible limits in wave propagation (Richards & Menke 1983; White *et al.* 1987; White, Sheng & Nair 1990), although presently it is unclear whether the common approach of treating the Earth as a self-averaged random medium is valid (Shapiro & Zien 1993).

As an alternative to statistical methods, deterministic approaches are a valuable tool for estimating local parameters by direct measurements. Such approaches require exact solutions for the scattering problem, but only a few exist for special cases.

Even though these cases are based on simplified geometries for the numerous shapes and sizes of inhomogeneities that are present in the Earth, they are difficult to implement, and hence solutions in terms of asymptotic approximations are developed. The assumptions used in the derivation of asymptotic solutions are usually expressed in the form of strong inequalities where some combination of parameters is assumed to be much less or much larger than unity. For instance, for the case of Rayleigh scattering it is assumed that the parameter kR, where k is the wavenumber of the incident wave and R is the radius of the scatterer, satisfies the condition $kR \ll 1$. In the same manner, for the case of linearizing the inverse problem, we assume 'very small' relative deviations of elastic parameters and density. Such assumptions are convenient at the stage of mathematical development, but they present problems when attempting to determine the actual bounds on parameters during application of the results. Indeed, in realistic situations while operating with parameters having finite values, there is always a problem in justifying the validity of the approximation and determining the accuracy of the solution. What is the actual difference between the exact solution and the approximation that has been used? What are the upper limits of the parameters that can be used and still retain a specified level of accuracy in the solution? For the case of Rayleigh scattering of elastic waves, it appears that the limits of the approximation have not yet been quantified. An additional problem occurs when more than one assumption is involved in that they may be contradictory. This is a possibility for the case of Rayleigh scattering ($\omega \rightarrow 0$) in the far field ($r \rightarrow \infty$), where the parameter ($\omega r/V_p$) is assumed to be large. The intention of the present paper is to investigate the accuracy of several asymptotic solutions and quantify the limits under which these approximations are applicable. We present the error for the application of the asymptotic solutions as a function of various parameters and estimate under which conditions a given approximation provides an acceptable solution to the scattering problem.

Recently, Korneev & Johnson (1993a,b) derived a solution for the scattering of an elastic P wave by a spherical inclusion of arbitrary contrast and developed asymptotic solutions for this problem. We investigate their low-frequency Rayleigh approximation which is valid for an arbitrary distance between the observation point and the inhomogeneity, and compare it to the solutions based on near-field and far-field approximations. We present the validity range for these limited approximations with respect to the distance of observation and discuss the relative contributions of the near-and far-field terms to the complete Rayleigh approximation. It should be noted here that, while these approximations were derived from the exact solution for a sphere, they depend only upon the volume of the scatterer and not upon its shape, and thus should be valid for the general class of inclusions with approximately equal dimensions.

The Rayleigh approximation can be used to model the scattering process of low-frequency waves by an inhomogeneity. A common goal in seismology is to determine the elastic properties of this inhomogeneity by inversion techniques. However, since the dependence of the solution on the elastic parameters is non-linear, the inversion of the data often is preceded by a linearization of the problem. For this purpose, we derive a linearized solution in terms of the elastic parameters and assess the error as a function of their perturbations. Furthermore, the improvement of the approximation by accounting for higher-order terms is investigated. The determination of the relative error is based on the parameter values of the inhomogeniety and the background medium. Often these values are unavailable, particularly in the planning stage of an experiment when anticipated errors play an important role. Therefore, we develop an equation for the approximate error due to linearization of the problem that is based entirely on the estimated parameter perturbations from the background values. Finally, we investigate the upper limit for the Rayleigh approximation ($kR \ll 1$) as a function of parameter perturbation.

2 RAYLEIGH APPROXIMATION FOR AN ELASTIC SPHERE OF ARBITRARY CONTRAST

A derivation of the exact scattering solution for a homogeneous elastic sphere was given by Korneev & Johnson (1993a,b). In their second paper they derive a low-frequency approximation for a spherical inclusion. However, because of its low-frequency range, this approximation simultaneously provides a solution for a wide range of arbitrarily-shaped 3-D structures. For reasons of clarity, we restate the exact solution again and follow their derivation of the low-frequency approximation.

The investigated scattering problem consists of an elastic inclusion defined by the parameters λ_1, μ_1 and ρ_1 (in the following, the index $\nu = 1$ denotes the medium of the inclusion) embedded in a homogeneous medium with constant parameters λ_2, μ_2 and ρ_2 (in the following, the index $\nu = 2$ refers to the background medium). The geometry for this situation is shown in Fig. 1. A joint Cartesian (x, y, z) and spherical (r, θ, ϕ) coordinate system with its origin at the centre of the inclusion is considered.

Throughout the paper, we will use an incident plane P wave of the form

$$\tilde{\mathbf{U}}_0 = e^{i\omega(t - z/V_{p_2})}\hat{\mathbf{z}} = \mathbf{U}_0 e^{i\omega t} \tag{1}$$

which is travelling in the background medium in a positive direction along the z axis. $\mathbf{U}_0$ denotes the Fourier transform of the incident wave. However, at the end of this section, we will provide a factor that accounts for an incident spherical wave generated by a point pressure source.

In the frequency domain, the total solution to the scattering problem can be written as a sum of the incident and the scattered fields:

$$\tilde{\mathbf{U}} = \mathbf{U}e^{i\omega t} = (\mathbf{U}_0 + \mathbf{U}_p + \mathbf{U}_s)e^{i\omega t} \tag{2}$$

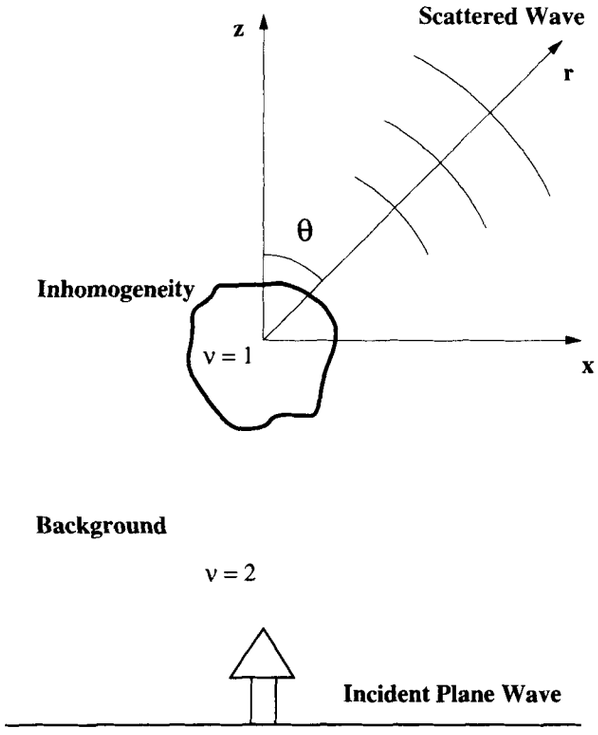

Figure 1. Geometry of the problem. The properties of the inhomogeneity and the background are denoted by $\nu = 1$ and $\nu = 2$, respectively. A plane wave is incident in the positive z direction, while the observation of the scattered wave is a function of $\boldsymbol{\theta}$ and $\mathbf{r}$.

where $\mathbf{U}_p$ and $\mathbf{U}_s$ denote the scattered P and S waves, respectively.

For the case of a plane P wave impinging upon a sphere, the total scattered fields can be represented as

$$\begin{aligned}\mathbf{U}_{sc} &= \mathbf{U}_p + \mathbf{U}_s \\ &= \sum_{l\geq 0} e^{-i\pi/2(l+1)}(2l+1)\left\{a_l\left[\left((l+1)\frac{h_l(k_p r)}{k_p r} - h_{l-1}(k_p r)\right)P_l(\cos\theta)\hat{\mathbf{r}} - \frac{h_l(k_p r)}{k_p r}\frac{\partial P_l(\cos\theta)}{\partial\theta}\hat{\boldsymbol{\theta}}\right]\right. \\ &\left. + b_l\left[l(l+1)\frac{h_l(k_s r)}{k_s r}P_l(\cos\theta)\hat{\mathbf{r}} + \left(h_{l-1}(k_s r) - \frac{h_l(k_s r)}{k_s r}\right)\frac{\partial P_l(\cos\theta)}{\partial\theta}\hat{\boldsymbol{\theta}}\right]\right\} \qquad (3)\end{aligned}$$

where $h_k(x)$ are spherical Hankel functions of the second kind and P_l are the Legendre functions. The coefficients a_l and b_l depend upon the properties of the sphere as well as the background medium. They also depend on the wavenumber of the scattered fields. For a detailed discussion of the derivation we refer to Korneev & Johnson (1993a).

For the development of the low-frequency approximation, we only use those terms of the exact solution that are of lowest degree in frequency. These terms (ω^3) are of third order and appear only in the first three coefficients ($l = 0, 1, 2$) of the exact solution.

$$\begin{aligned}a_0 &= i\frac{\xi^3}{6}\frac{\frac{3}{2}(\lambda_1 - \lambda_2) + \mu_1 - \mu_2}{\frac{1}{2}(\frac{3}{2}\lambda_1 + \mu_1) + \mu_2} \\ a_1 &= -i\frac{\xi^3}{9}\left(\frac{\rho_1}{\rho_2} - 1\right), \qquad b_1 = i\frac{\eta^3}{9}\left(\frac{\rho_1}{\rho_2} - 1\right) \qquad (4) \\ a_2 &= i\xi^3\frac{4}{45}\left(\frac{\mu_1}{\mu_2} - 1\right)\frac{\gamma^2}{D}, \qquad b_2 = -i\eta^3\frac{2}{45}\left(\frac{\mu_1}{\mu_2} - 1\right)\frac{\gamma}{D}\end{aligned}$$

with

$$\begin{aligned}V_{p_\nu} &= \sqrt{\frac{\lambda_\nu + 2\mu_\nu}{\rho_\nu}}, \qquad V_{s_\nu} = \sqrt{\frac{\mu_\nu}{\rho_\nu}}, \qquad k_p = \frac{\omega}{V_{p_2}}, \qquad k_s = \frac{\omega}{V_{s_2}} \\ \xi &= k_p R, \qquad \eta = k_s R \\ \gamma &= \frac{V_{s_2}}{V_{p_2}}, \qquad D = 1 + \frac{2}{15}\left(\frac{\mu_1}{\mu_2} - 1\right)(3 + 2\gamma^2). \qquad (5)\end{aligned}$$

Thus, we obtain a low-frequency approximation with no restrictions upon the elastic parameters as:

$$\mathbf{U}_{sc} = \mathbf{U}_p + \mathbf{U}_s$$

with

$$\mathbf{U}_p = (\mathbf{U}_p(\theta))_r\hat{\mathbf{r}} + (\mathbf{U}_p(\theta))_\theta\hat{\boldsymbol{\theta}}$$

$$= A\left\{\left[-\frac{1}{2}\frac{\frac{3}{2}(\lambda_1-\lambda_2)+\mu_1-\mu_2}{\frac{1}{2}(\frac{3}{2}\lambda_1+\mu_1)+\mu_2}W^p_{0r}(Z_p)+\left(\frac{\rho_1}{\rho_2}-1\right)W^p_{1r}(Z_p)\cos\theta+\frac{2}{3}\left(\frac{\mu_1}{\mu_2}-1\right)\frac{\gamma^2}{D}W^p_{2r}(Z_p)(1-3\cos^2\theta)\right]\hat{\mathbf{r}}\right.$$

$$\left.-\left[\left(\frac{\rho_1}{\rho_2}-1\right)W^p_{1\theta}(Z_p)\sin\theta+2\left(\frac{\mu_1}{\mu_2}-1\right)\frac{\gamma^2}{D}W^p_{2\theta}(Z_p)\sin 2\theta\right]\hat{\boldsymbol{\theta}}\right\}. \tag{6a}$$

$$\mathbf{U}_s = (\mathbf{U}_s(\theta))_r\hat{\mathbf{r}} + (\mathbf{U}_s(\theta))_\theta\hat{\boldsymbol{\theta}}$$

$$= B\left\{\left[2\left(\frac{\rho_1}{\rho_2}-1\right)W^s_{1r}(Z_s)\cos\theta+2\left(\frac{\mu_1}{\mu_2}-1\right)\frac{\gamma}{D}W^s_{2r}(Z_s)(3\cos^2\theta-1)\right]\hat{\mathbf{r}}\right.$$

$$\left.+\left[-\left(\frac{\rho_1}{\rho_2}-1\right)W^s_{1\theta}(Z_s)\sin\theta+\left(\frac{\mu_1}{\mu_2}-1\right)\frac{\gamma}{D}W^s_{2\theta}(Z_s)\sin 2\theta\right]\hat{\boldsymbol{\theta}}\right\}. \tag{6b}$$

The new functions are defined as follows

$$A = k_p^2\frac{V}{4\pi}\frac{e^{-ik_pr}}{r}, \qquad B = k_s^2\frac{V}{4\pi}\frac{e^{-ik_sr}}{r}, \tag{7}$$

where V is the volume of the inclusion, and

$$W^p_{0r}(Z_p) = 1-\frac{i}{Z_p}$$

$$W^p_{1r}(Z_p) = 1-2\frac{1+iZ_p}{Z_p^2}, \quad W^p_{2r}(Z_p) = 1+\frac{9i-4iZ_p^2-9Z_p}{Z_p^3}$$

$$W^s_{1\theta}(Z_s) = 1-\frac{1+iZ_s}{Z_s^2}, \quad W^s_{2\theta}(Z_s) = 1+3\frac{2i-iZ_s^2-2Z_s}{Z_s^3}$$

$$W^p_{1\theta}(Z_p) = \frac{1+iZ_p}{Z_p^2}, \quad W^p_{2\theta}(Z_p) = \frac{3i-iZ_p^2-3Z_p}{Z_p^3}$$

$$W^s_{1r}(Z_s) = \frac{1+iZ_s}{Z_s^2}, \quad W^s_{2r}(Z_s) = \frac{3i-iZ_s^2-3Z_s}{Z_s^3}, \tag{8}$$

with

$$Z_p = k_pr = \frac{\omega r}{V_{p2}}, \qquad Z_s = k_sr = \frac{\omega r}{V_{s2}}. \tag{9}$$

The above approximation has used the lowest degree in frequency only, and is based on the assumption that

$$k_{\max}R = \frac{\omega R}{V_{\min}} \ll 1, \tag{10}$$

where $V_{\min}$ denotes the minimum velocity and $k_{\max}$ represents the corresponding wavenumber. This result, generally known as the Rayleigh approximation, does not depend upon the shape of the inclusion but only upon its volume.

The W functions in eq. (8) contain the distance dependence of the observation point from the centre of the sphere and are valid for all values of $r \geq R$. Thus, the expression in eq. (6) is a complete solution containing near- and far-field contributions. From this solution it is evident that the P wave of the scattered field contains a contribution in the $\hat{\boldsymbol{\theta}}$ direction, while the S wave contains a factor in the $\hat{\mathbf{r}}$ direction. Thus, the P and S waves are not decoupled and their polarization is complicated in the near field. However, as the distance of observation increases, the relative contributions of the W functions change in such a way that the solution takes on the form of the far-field approximation.

To obtain the far-field approximation, we have to satisfy the following conditions for the W functions in their limits:

$$|W^p_{0r}(Z_p)| \approx 1, \quad |W^p_{1r}(Z_p)| \approx 1, \quad |W^p_{2r}(Z_p)| \approx 1, \quad |W^s_{1\theta}(Z_s)| \approx 1, \quad |W^s_{2\theta}(Z_s)| \approx 1 \tag{11}$$

$$|W^p_{1\theta}(Z_p)| \approx 0, \quad |W^p_{2\theta}(Z_p)| \approx 0, \quad |W^s_{1r}(Z_s)| \approx 0, \quad |W^s_{2r}(Z_s)| \approx 0. \tag{12}$$

In this limit, the scattered field can be divided into an $\hat{\mathbf{r}}$ and a $\hat{\boldsymbol{\theta}}$ component, both revealing a $1/r$ dependence for scattered waves in the far field:

$$\mathbf{U}_p = k_p^2 \frac{V}{4\pi} \frac{e^{-ik_p r}}{r} \left\{ -\frac{1}{2} \frac{\frac{3}{2}(\lambda_1 - \lambda_2) + \mu_1 - \mu_2}{\frac{1}{2}(\frac{3}{2}\lambda_1 + \mu_1) + \mu_2} + \left(\frac{\rho_1}{\rho_2} - 1\right) \cos\theta + \frac{2}{3}\left(\frac{\mu_1}{\mu_2} - 1\right) \frac{\gamma^2}{D}(1 - 3\cos^2\theta) \right\} \hat{\mathbf{r}} \tag{13a}$$

$$\mathbf{U}_s = k_s^2 \frac{V}{4\pi} \frac{e^{-ik_s r}}{r} \left\{ -\left(\frac{\rho_1}{\rho_2} - 1\right) \sin\theta + \left(\frac{\mu_1}{\mu_2} - 1\right) \frac{\gamma}{D} \sin 2\theta \right\} \hat{\boldsymbol{\theta}}. \tag{13b}$$

The natural polarization in the $\hat{\mathbf{r}}$- and $\hat{\boldsymbol{\theta}}$-direction for the P and S waves, respectively, is evident.

The effect on the amplitude of the scattered field of the ratio between R and the wavelength λ_p of the incident P wave can easily be addressed by putting the solution (6) in the form

$$\mathbf{U}_p + \mathbf{U}_s = (k_p R)^3 \mathbf{F}(Z_p, \theta) = \left(2\pi \frac{R}{\lambda_p}\right)^3 \mathbf{F}(Z_p, \theta) \tag{14}$$

(using $Z_p = \gamma Z_s$) where the function $\mathbf{F}(Z_p, \theta)$ also depends upon the parameter perturbations, but does not depend on the radius R of the inclusion. Thus, when $R \to \lambda_p$, the amplitudes increase until a maximum is reached for the Rayleigh limit $(k_p R)_{\text{lim}}$.

In the near field, where $Z_p \ll 1.0$ and $Z_s \ll 1.0$ the P and S components of the scattered field may be combined to form an asymptotic solution depending on both $\hat{\mathbf{r}}$ and $\hat{\boldsymbol{\theta}}$, by expanding $e^{-ik_p r}$ and $e^{-ik_s r}$ in eq. (7) and keeping only the lowest degree in Z_p.

$$\mathbf{U}_{sc} = \frac{V}{4\pi r^3} \left\{ \left[\frac{i}{2} \frac{\frac{3}{2}(\lambda_1 - \lambda_2) + \mu_1 - \mu_2}{\frac{1}{2}(\frac{3}{2}\lambda_1 + \mu_1) + \mu_2} Z_p + \frac{1}{\gamma^2}\left(\frac{\rho_1}{\rho_2} - 1\right) Z_p^2 \cos\theta + i\left(1 - \frac{\gamma^2}{3}\right)\left(\frac{\mu_1}{\mu_2} - 1\right) \frac{Z_p}{D}(3\cos^2\theta - 1) \right] \hat{\mathbf{r}} \right.$$
$$\left. - \left[\frac{(1+\gamma^2)}{2\gamma^2}\left(\frac{\rho_1}{\rho_2} - 1\right) Z_p^2 \sin\theta + i\gamma^2 \left(\frac{\mu_1}{\mu_2} - 1\right) \frac{Z_p}{D} \sin 2\theta \right] \hat{\boldsymbol{\theta}} \right\}. \tag{15}$$

With the definitions for Z_p and Z_s in eq. (9), it becomes apparent that the amplitude for the near-field approximation contains components which are proportional to $1/r$ and $1/r^2$. The sum of the $\hat{\mathbf{r}}$ and $\hat{\boldsymbol{\theta}}$ components indicates the complicated polarization, as the P and S wave are not decoupled yet.

So far, we have treated the scattering problem considering an incident plane P wave with a source located at infinity. However, the problem can as well be addressed for the case of an inhomogeneity in the near or far field of a point pressure source exciting a spherical P wave

$$\mathbf{U}_0 = -\nabla \frac{e^{-ik_p|\mathbf{r} - \mathbf{r}_0|}}{|\mathbf{r} - \mathbf{r}_0|}, \tag{16}$$

where r_0 is the distance between the point source and the centre of the inclusion. The consideration of a spherical incident wave introduces additional functions for the distance dependence of the scattered field of the form

$$C_0 = q$$

$$C_1 = \frac{Z_{p0} - i}{Z_{p0}} q$$

$$C_2 = \frac{Z_{p0}^2 - 3iZ_{p0} - 3}{Z_{p0}^2} q, \tag{17}$$

with

$$q = \frac{k_p}{r_0}, \qquad Z_{p0} = k_p r_0 = \frac{\omega r_0}{V_{p2}}.$$

The C_l have to be multiplied onto those W_l functions in eq. (8) that have the same degree in l to provide the correct distance-dependent functions for the case of a single-point pressure source at an arbitrary distance from the inhomogeneity. However, in this study we address the problem of an incident plane P wave only. This restriction permits all of the displacement fields to be represented in terms of unitless values for the purpose of simplicity in presenting numerical results.

3 COMPARISON BETWEEN LOW-FREQUENCY TOTAL SOLUTION AND THE APPROXIMATIONS IN THE NEAR AND FAR FIELDS

For the comparison of the various approximations listed above, we compute the scattered amplitude for a given spherical inclusion with radius R along a profile of observation extending from $r = R$ (near field) to $r \gg R$ (far field). The profiles are computed for various scattering angles between $\theta = 0°$ and $\theta = 180°$ (symmetry exists along the 0°–180° axis of incidence) to present a qualitative view of the angular dependence. The results are computed for an inhomogeneity with a 10 per cent increase in V_p and V_s velocity as well as density with respect to the background. The structure (eq. 14) of the scattered field makes it possible to investigate the unitless function $\mathbf{F}$ independently of the radius R of the inclusion, thus producing results with more universal application. In Fig. 2(a,b,c) absolute values of the r-component of $\mathbf{F}(Z_p, \theta)$ are plotted as functions of $Z_p = k_p r$ of the incident wave for three different angles $\theta = 0°$(a), 90°(b), 180°(c). In order to compare results of a different geometry with these curves, the minimum value of the parameter $k_p R$ has to be determined for the new geometry, and subsequently the normalized amplitudes to the right of the new limit on the abscissa will be comparable after multiplication by the corresponding value of $(k_p R)^3$. This minimum should be equal to or less than the Rayleigh limit $(k_p R)_{\text{lim}}$, which depends upon the parameter perturbations. A detailed discussion on the validity range of the Rayleigh limit is presented in Section 5.

For each value of θ in Fig. 2(a,b,c) three curves are shown, representing the $\hat{\mathbf{r}}$ component of the total field (solid line, eq. 6), the near field (dashed line, eq. 15), and the far field (dotted line, eq. 13) of the Rayleigh approximation. The graphs are plotted using a logarithmic scale for both axes. Thus, the far-field solution with a distance dependence of $1/r$ appears as a straight line with a slope of -1, whereas the near-field solution revealing both a $1/r$ and $1/r^2$ dependence produces two constant slopes. In the very near field the $1/r^2$ term is dominant, creating a slope of -2, while for larger distances the dominance of the $1/r$ term is apparent by a change in slope to -1. The transition between these two slopes is defined by contributions from both factors. However, the application of the approximations at various distances of observation requires a careful investigation of their validity range. All curves are computed between $k_p r = 10^{-2}$ and $k_p r = 10^3$, although only the total field is valid for the whole range, as we found from comparison with the exact solution for the sphere. The near-field solution is applicable in the vicinity of the inhomogeneity, whereas the far field yields correct values at a greater distance from the inhomogeneity only. (This is supported by Fig. 2a.) The total field solution coincides very well with the near-field solution for small values of $k_p r$, whereas the discrepancy becomes larger for greater distances of observation. Similarly, it differs from the far-field solution in the near field, while asymptotically, the two solutions merge in the far field. The oscillatory nature of the total solution in the $\hat{\mathbf{r}}$ and the $\hat{\boldsymbol{\theta}}$ components is based on the near-field contribution of the S wave ($\mathbf{k}_s$ vector in the $\hat{\mathbf{r}}$ component) and P wave ($\mathbf{k}_p$ vector in the $\hat{\boldsymbol{\theta}}$ component), respectively. The interference between both components is present in the near field only and decreases in the far field.

The most intriguing result is the large-amplitude difference between the total and the far-field solution of magnitude ~300 for the very near field $k_p r = 10^{-2}$. This difference decays continuously until good agreement is reached at a distance of approximately $k_p r \approx 4\pi (r \approx 2\lambda)$. Between $k_p r = 10^{-2}$ and $k_p r \approx 4\pi/10$ ($r \approx 0.2\lambda$), the near field provides a better approximation than the far-field solution. In between these distances ($0.2\lambda < r < 2\lambda$), a range that we refer to as the mid-field, both solutions present an alternating fit to the total field because of its oscillatory behaviour. Fig. 2(a) presents pure forward scattering ($\theta = 0°$), while Figs 2(b) and (c) show the results for a scattering angle of $\theta = 90°$ and $\theta = 180°$ (backscattering), respectively. It is evident that the main features described above still apply in these cases, although the amplitude difference between total and far fields for $r = R$ decreases by one order of magnitude for $\theta = 90°$, before it regains the initial value for $\theta = 180°$. For the scattering angle of $\theta = 90°$, a drop in amplitude of the near-field solution below the values of the far-field solution is noticeable yet without bearing as the solution is not valid in this range.

The $\hat{\boldsymbol{\theta}}$ components of the same fields are presented in Figs 3(a)–(c). Because the amplitude of the $\hat{\boldsymbol{\theta}}$ component is zero for $\theta = 0°$ and $\theta = 180°$, we show the results for $\theta = 45°$, $\theta = 90°$ and $\theta = 135°$. Again, the total field coincides well with the near- and the far-field solutions in the near and far-field ranges, respectively. However, it is evident that the amplitude difference in the near field decreases to a factor of 15 for $\theta = 45°$ and $\theta = 135°$, and shows no significant difference for $\theta = 90°$, while the amplitudes are slightly larger for the far-field solution. The mid-field region is characterized by a misfit for both near-field and far-field solutions, although the total field solution reveals less oscillations.

The oscillatory nature of the total field solution causes similar oscillations of the relative error between the total field and the far- or near-field solutions. Because of this it is useful to define the mean value of the error as the smooth trend through the residuals, which minimizes the effect of the rapidly fluctuating values. For the relative error in the $\hat{\mathbf{r}}$ component, we found such a mean value to be 15 per cent at a distance of 2λ. However, the oscillations around this value can be as high as 35 per cent and as low as 2 per cent. At a distance of 10λ, for example, the mean error has decreased to 5 per cent with variations between 8 per cent and 2 per cent. The values for the $\hat{\boldsymbol{\theta}}$ component reveal a smaller error over the entire distance of observation. At 2λ, the mean value of the relative error is 2 per cent, with fluctuations between 4 per cent and 0 per cent, and this decreases gradually with increasing distance of observation.

The comparison between the total- and far-field solutions indicates the advantage of near-field components in the total-field solution. The high amplitudes of the scattered waves in the near-field suggest an improvement for the determination of the

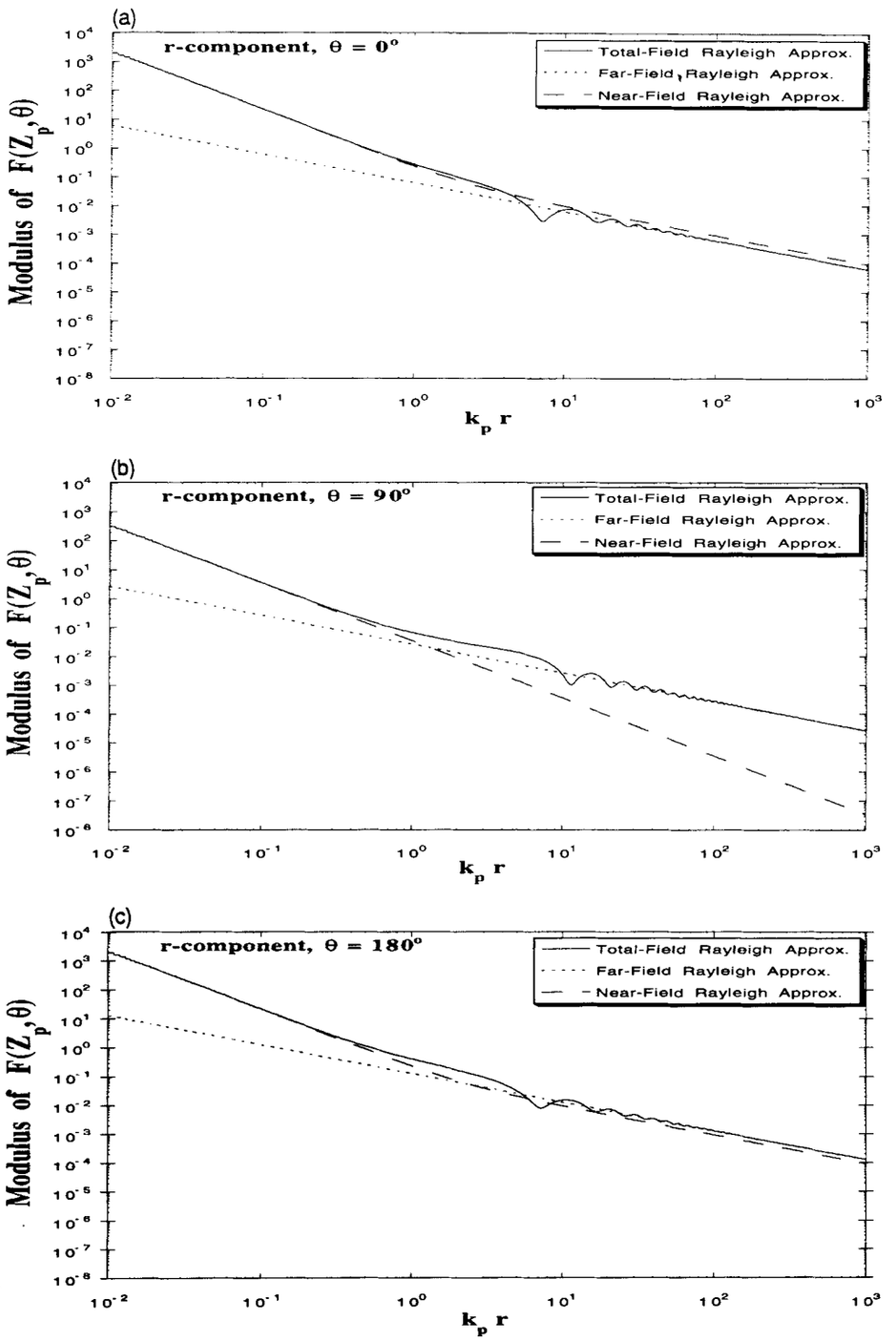

Figure 2. Normalized modulus of amplitude factor $\mathbf{F}(Z_p, \theta)$ (eq. 14). Radial component of the low-frequency scattered fields for a high velocity and high density inclusion of +10 per cent.

elastic properties, under the assumption that corrections for the incident field can be applied. Thus the deployment of recording instrumentation in the vicinity of inhomogeneities together with the observation of the incident field could improve the results for inverting scattered energy. In addition the limit for the validity of the far-field solution indicates that for an observation distance less than 2λ, this solution produces wrong results, while it can be applied to distances greater than 2λ.

The presented results are computed for an inhomogeneity with a 10 per cent increase in V_p and V_s velocities as well as in its density with respect to the background. Because we compute the modulus of the amplitudes, investigations of a negative perturbation produce the same shape and relations of the amplitude curves as for an equal-magnitude positive perturbation. To determine the sign of the perturbation, the separate use of real and imaginary part is more appropriate. However, the

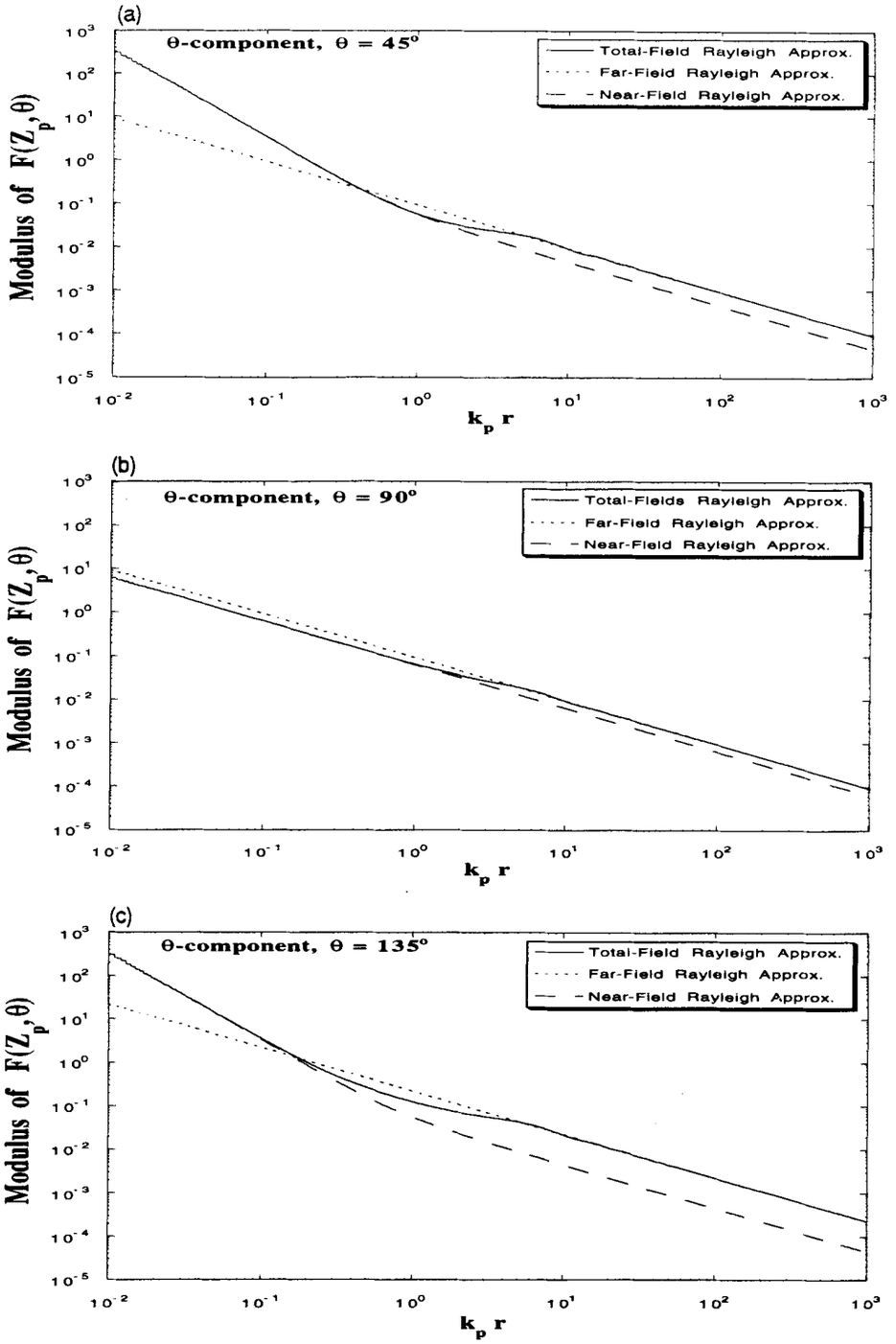

Figure 3. Normalized modulus of amplitude factor $\mathbf{F}(Z_p, \theta)$ (eq. 14). Azimuthal component of the low-frequency scattered fields for a high-velocity and high-density inclusion of +10 per cent.

investigation of scattering diagrams as a function of combinations of parameter perturbations is beyond the purpose of this paper, and we refer to works by Sato (1984), Wu & Aki (1985), and Tarantola (1986).

4 EXTENSION AND EVALUATION OF THE RAYLEIGH–BORN APPROXIMATION

Thus far, we treated scattering solutions for arbitrary contrast in the elastic parameters only. In eq. (4) the coefficients are non-linear in terms of the elastic parameters λ and μ. This can be problematic, if a solution for the inversion of the scattering

problem in terms of the elastic parameters is sought. A common practice, therefore, is to solve the linearized inversion problem. This linearization is often referred to as the Born approximation. The actual conditions for the validity of the Born approximation include the size of the inclusion, the perturbation of its elastic parameters with respect to the background, and the phase shift between different scattered phases (Hudson & Heritage 1981). In the Rayleigh scattering regime, the wavelength is large compared to the scatterer size, and, for the case of a weak inhomogeneity, the consideration of a possible phase shift can be neglected. Thus, for this case, the Born approximation is valid, and is often referred to as the Rayleigh–Born approximation. To linearize the problem, the coefficients are expressed in a converging binomial series expansion assuming the perturbations in the parameters are smaller than the background values. The approximate solution is found by keeping the linear term of the series expansion while disregarding higher orders. This step is valid only for small perturbations:

$$\frac{|\delta\lambda|}{\lambda_2} = \frac{|\lambda_1 - \lambda_2|}{\lambda_2} \ll 1, \qquad \frac{|\delta\mu|}{\mu_2} = \frac{|\mu_1 - \mu_2|}{\mu_2} \ll 1, \qquad \frac{|\delta\rho|}{\rho_2} = \frac{|\rho_1 - \rho_2|}{\rho_2} \ll 1. \tag{18}$$

Expanding the coefficients in eq. (4) in terms of the elastic parameters and keeping the first terms only yields a linearized solution to the scattering problem which has the form

$$\mathbf{U}_{sc}^{(1)} = \mathbf{U}_p^{(1)} + \mathbf{U}_s^{(1)}$$

with

$$\mathbf{U}_p^{(1)} = A\left\{\left[-\frac{1}{2}\frac{\frac{3}{2}\delta\lambda + \delta\mu}{\frac{1}{2}(\frac{3}{2}\lambda_2 + \mu_2) + \mu_2} W_{0r}^p(Z_p) + \frac{\delta\rho}{\rho_2} W_{1r}^p(Z_p)\cos\theta + \frac{2}{3}\frac{\delta\mu}{\mu_2}\gamma^2 W_{2r}^p(Z_p)(1 - 3\cos^2\theta)\right]\hat{\mathbf{r}}\right.$$

$$\left. - \left[\frac{\delta\rho}{\rho_2} W_{1\theta}^p(Z_p)\sin\theta + 2\frac{\delta\mu}{\mu_2}\gamma^2 W_{2\theta}^p(Z_p)\sin 2\theta\right]\hat{\boldsymbol{\theta}}\right\}. \tag{19a}$$

$$\mathbf{U}_s^{(1)} = B\left\{\left[2\frac{\delta\rho}{\rho_2} W_{1r}^s(Z_s)\cos\theta + 2\frac{\delta\mu}{\mu_2}\gamma W_{2r}^s(Z_s)(3\cos^2\theta - 1)\right]\hat{\mathbf{r}}\right.$$

$$\left. + \left[-\frac{\delta\rho}{\rho_2} W_{1\theta}^s(Z_s)\sin\theta + \frac{\delta\mu}{\mu_2}\gamma W_{2\theta}^s(Z_s)\sin 2\theta\right]\hat{\boldsymbol{\theta}}\right\}. \tag{19b}$$

In order to evaluate the error made by applying the linearized solution, we go a step further and use the linear and the quadratic term of the expansion for the coefficients in eq. (4) and derive a more exact approximation to the non-linear solution which we will refer to as the quadratic approximation. This gives

$$\mathbf{U}_{sc}^{(2)} = \mathbf{U}_p^{(2)} + \mathbf{U}_s^{(2)}$$

where

$$\mathbf{U}_p^{(2)} = A\left\{\left[-\frac{1}{2}\left(\frac{\frac{3}{2}\delta\lambda + \delta\mu}{\frac{1}{2}(\frac{3}{2}\lambda_2 + \mu_2) + \mu_2} - \frac{1}{2}\frac{(\frac{3}{2}\delta\lambda + \delta\mu)^2}{\frac{1}{2}(\frac{3}{2}\lambda_2 + \mu_2) + \mu_2)^2}\right) W_{0r}^p(Z_p) + \frac{\delta\rho}{\rho_2} W_{1r}^p(Z_p)\cos\theta\right.$$

$$\left. + \frac{2}{3}\left(\frac{\delta\mu}{\mu_2} - \frac{2}{15}\left(\frac{\delta\mu}{\mu_2}\right)^2(3 + 2\gamma^2)\right)\gamma^2 W_{2r}^p(Z_p)(1 - 3\cos^2\theta)\right]\hat{\mathbf{r}}$$

$$\left. - \left[\frac{\delta\rho}{\rho_2} W_{1\theta}^p(Z_p)\sin\theta + 2\left(\frac{\delta\mu}{\mu_2} - \frac{2}{15}\left(\frac{\delta\mu}{\mu_2}\right)^2(3 + 2\gamma^2)\right)\gamma^2 W_{2\theta}^p(Z_p)\sin 2\theta\right]\hat{\boldsymbol{\theta}}\right\}. \tag{20a}$$

$$\mathbf{U}_s^{(2)} = B\left\{\left[2\frac{\delta\rho}{\rho_2} W_{1r}^s(Z_s)\cos\theta + 2\left(\frac{\delta\mu}{\mu_2} - \frac{2}{15}\left(\frac{\delta\mu}{\mu_2}\right)^2(3 + 2\gamma^2)\right)\gamma W_{2r}^s(Z_s)(3\cos^2\theta - 1)\right]\hat{\mathbf{r}}\right.$$

$$\left. + \left[-\frac{\delta\rho}{\rho_2} W_{1\theta}^s(Z_s)\sin\theta + \left(\frac{\delta\mu}{\mu_2} - \frac{2}{15}\left(\frac{\delta\mu}{\mu_2}\right)^2(3 + 2\gamma^2)\right)\gamma W_{2\theta}^s(Z_s)\sin 2\theta\right]\hat{\boldsymbol{\theta}}\right\}. \tag{20b}$$

Eqs (6), (19) and (20) are the basis for the evaluation of the error in approximating the non-linear solution. The evaluations are undertaken in the far field of the inhomogeneity, allowing the application of the commonly used far-field approximation. First, we evaluate the error in terms of the scattering angle to investigate the possible effects of the scattering direction. Therefore, we determine the amplitude of the scattered field for all angles between 0° and 360° using the three

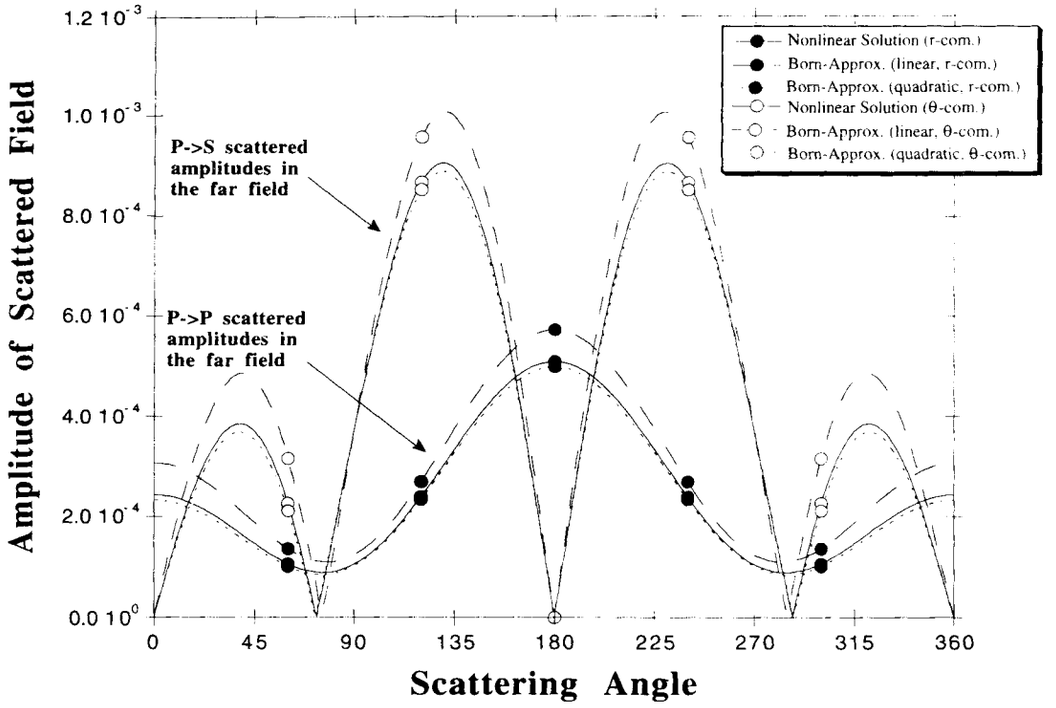

Figure 4. Amplitudes of scattered fields as a function of scattering angle.

equations mentioned above. The result is given in Fig. 4. For both components, the amplitude values of the linear approximation exceed the non-linear solution, while the quadratic approximation underestimates it. This is caused by the alternating sign in the series expansion with increasing order.

A problem for the estimation of the relative error between the approximations and the non-linear solution for every scattering angle arises from the vanishing amplitude values at $\theta \approx 0°$, 75°, 180°, 285°, 360°. These singularities produce unphysically high values for the relative error. Therefore, we will relate the error in the $\hat{\mathbf{r}}$ and $\hat{\boldsymbol{\theta}}$ component to the mean square amplitude

$$\overline{(\mathbf{U}_{sc})_c^2} = \frac{1}{2}\int_0^\pi |U_{sc}(\theta)|_c^2 \sin\theta \, d\theta. \tag{21}$$

Here, $c = r$, θ denotes the components of the scattered wave. Hence the relative error becomes

$$\Delta e_c^{(\varepsilon)} = \left(\frac{(U_{sc}^{(\varepsilon)}(\theta) - U_{sc}(\theta))_c^2}{\overline{(U_{sc})_c^2}}\right)^{1/2} \tag{22}$$

where $\varepsilon = 1,2$ represents the linear and quadratic Rayleigh–Born approximation, while $U_{sc}^{(\varepsilon)}(\theta)$ and $U_{sc}(\theta)$ denote the scattered field of eqs (19), (20) and (6), respectively. Thus, we normalize the error for each component by the average scattered amplitude of the same component. Fig. 5 reveals the results. For the $\hat{\mathbf{r}}$ component, a relatively smooth distribution of the error can be seen. The scattering problem is symmetric along the 0°–180° axis. One evident feature is the decrease of the error between the forward and the 90° scattering direction by a factor of ~3. Further, it can be seen that for this particular example of a velocity and density perturbation of +10 per cent, the introduction of the quadratic term in the series expansion reduces the error compared to the linear approximation by a factor of more than 5. The same improvement is found for the $\hat{\boldsymbol{\theta}}$ component. Distinct lobes at angles of approximately 45° to both sides of the axis of wave incidence are visible. For both components no particular difference between forward and backscattering is evident. This representation of the error reveals the strong dependence on the scattering angle and provides some insight into the improvement to be gained by taking into account the quadratic term in the series expansion.

Next, in order to estimate the error as a function of perturbation in the elastic parameters, we integrate the difference between the Rayleigh–Born and the non-linear approximations over all scattering angles θ,

$$\overline{(\mathbf{U}_{sc}^{(\varepsilon)} - \mathbf{U}_{sc})^2} = \frac{1}{2}\int_0^\pi |U_{sc}^{(\varepsilon)}(\theta) - U_{sc}(\theta)|^2 \sin\theta \, d\theta, \tag{23}$$

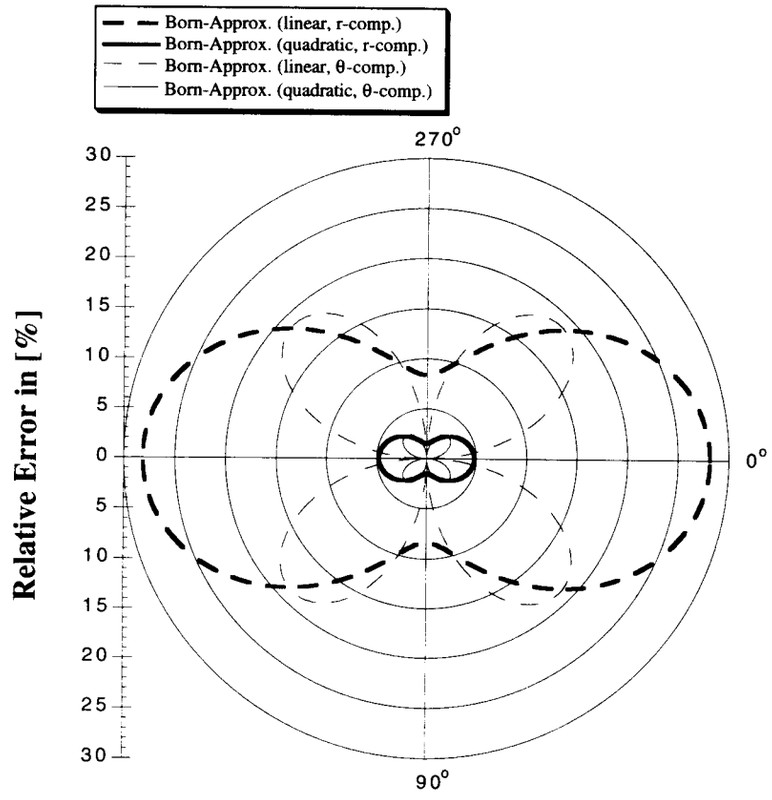

Figure 5. Relative error of the radial and azimuthal components of the linear and quadratic Rayleigh–Born approximations.

and relate it to the non-linear approximate solution integrated over all scattering angles θ.

$$\overline{\mathbf{U}_{sc}^2} = \frac{1}{2}\int_0^{\pi} |U_{sc}|^2 \sin\theta \, d\theta. \tag{24}$$

This allows us to compare the total average scattered amplitude for the non-linear and the approximate solutions and investigate it as a function of parameter perturbation. Hence the error becomes

$$\Delta e^{(e)} = \left(\frac{\overline{(U_{sc}^{(e)} - U_{sc})^2}}{\overline{U_{sc}^2}}\right)^{1/2}, \tag{25}$$

where the notation is equivalent to eqs (21) and (22). The result is shown in Fig. 6 for positive and negative parameter perturbations in λ, μ and ρ. The quadratic approximation reveals a smaller error compared to the linear approximation over the entire range for both cases of a positive and negative perturbation. However, the best improvement is achieved for perturbations less than 20 per cent. While −100 per cent constitutes a lower limit for the error, it was found that above a perturbation of +200 per cent, the error for the linear approximation becomes less than for the quadratic approximation (although physically this is an acceptable statement, mathematically the extension beyond +100 per cent is incorrect, since the assumption for the series expansion of the elastic parameters (eq. 18) was that the absolute value of the relative parameter perturbation remains smaller than one).

It should be noted that the solution in eq. (6) depends linearly on the perturbation in density. Therefore, the scattering problem for an inhomogeneity with a change in density only can be exactly described by the linear approximation in eq. (19).

The difference in the errors between the linear and quadratic Rayleigh–Born approximations can be used in the inversion of a linearized problem. After the first iteration of the inversion, the quadratic Rayleigh–Born approximation is computed and the difference from the linear approximation can be applied to adjust the first preliminary result. The corrected result will be the input for the second iteration. This scheme, which should ensure a faster converging solution to the problem of inverting for the parameters of a scatterer, is the topic of current investigation.

In the following, we present a quantitative estimation of the relative error of the linear approximation based purely on the relative perturbations in the elastic parameters from the background values. This provides an important estimate for the error

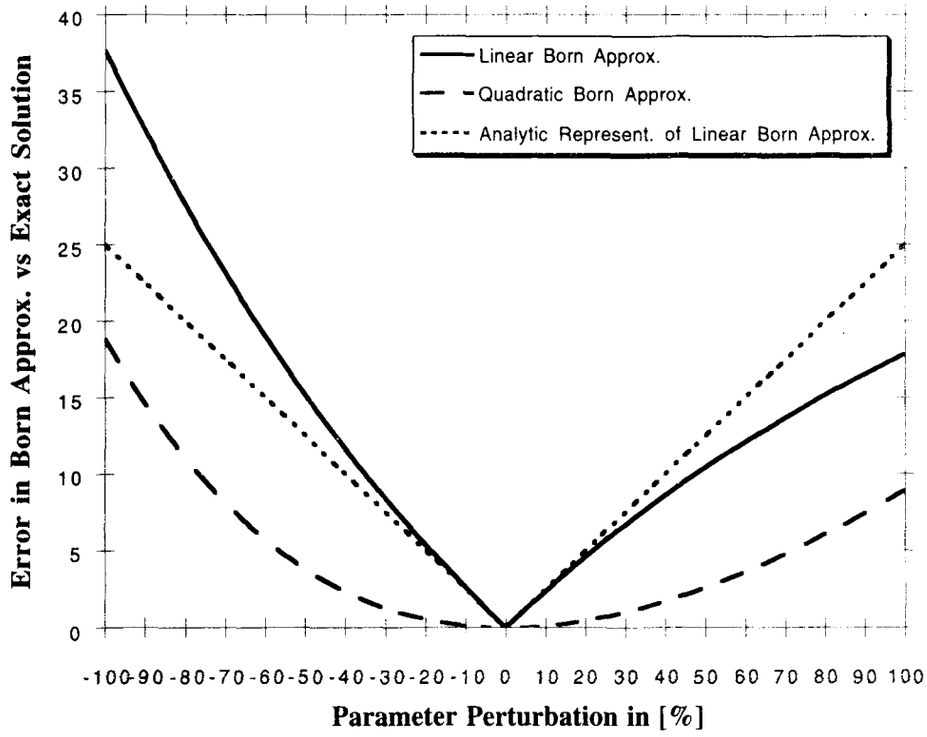

Figure 6. Relative average error of the linear and quadratic Rayleigh–Born approximations as a function of parameter perturbation.

due to linearization of an experiment where no absolute values are available, except for assumed perturbations of the inhomogeneity from the background. The error is based on the equation (25):

$$\Delta e^{(1)} = \left(\frac{\overline{(U_{sc}^{(1)} - U_{sc})^2}}{\overline{U_{sc}^2}} \right)^{1/2} \approx \left(\frac{\overline{(U_{sc}^{(1)} - U_{sc}^{(2)})^2}}{\overline{U_{sc}^{(1)2}}} \right)^{1/2}. \tag{26}$$

This has the advantage that only perturbation terms of the elastic parameters remain in the resulting equation. Assuming equal perturbations for $\delta\lambda/\lambda_2$ and $\delta\mu/\mu_2$,

$$\frac{\delta\lambda}{\lambda_2} = C, \quad \frac{\delta\mu}{\mu_2} = C, \quad \frac{\delta\rho}{\rho_2} = nC, \quad \text{and} \quad \gamma = \frac{V_s}{V_p} = \sqrt{\frac{1}{3}}, \tag{27}$$

we find

$$\Delta e^{(1)} = \frac{|C|}{2\sqrt{3n^2 + 1}}. \tag{28}$$

Thus for the case of similar perturbations in the density and the elastic parameters ($n = 1$) this yields $C/4$, whereas no density contrast ($n = 0$) produces an error of $C/2$. The dependence of this error on the perturbation in elastic parameters is shown in Fig. 6 (dashed line). A good agreement between the linear approximation and the estimated error is found up to a parameter perturbation of 20 per cent. The derived equation provides a means to estimate the minimum error in the total averaged scattered amplitude due to the linearization of the problem. It should be mentioned that for the case of an inversion, additional errors, associated with ill conditioning of the experiment and poor signal-to-noise ratios, for example, will increase the total error for the estimated parameters of the inclusion.

5 INVESTIGATION AND EVALUATION OF THE RAYLEIGH LIMIT

The Rayleigh approximation generally is based on the assumption that the parameter $k_p R$ is small compared to 1,

$$k_p R = \frac{\omega R}{V_p} \ll 1, \tag{29}$$

although the actual magnitude of the limit is not known. The value of $k_p R$ depends not only on the wavelength, the velocity of the background, and the dimensions of the scatterer, but also on the perturbations in the elastic parameters from the

background values. Therefore, we investigate the Rayleigh limit of k_pR as a function of perturbation in the elastic parameters. For a given perturbation, we compute, for a given value of k_pR, the average square amplitude over all scattering angles for the exact solution for the sphere (eq. 3) and for the Rayleigh approximation in the far field (eq. 13). The two solutions tend to deviate with increasing k_pR for a fixed perturbation value. We determine the Rayleigh limit from the value of k_pR that is reached for a predefined maximum deviation of these two solutions. The result is shown in Fig. 7. We set the maximum deviation between the two solutions to 5 per cent, 10 per cent and 20 per cent. The parameter perturbation was chosen to vary, when possible, −100 per cent and +300 per cent. Three different relations between the perturbations of elastic moduli and

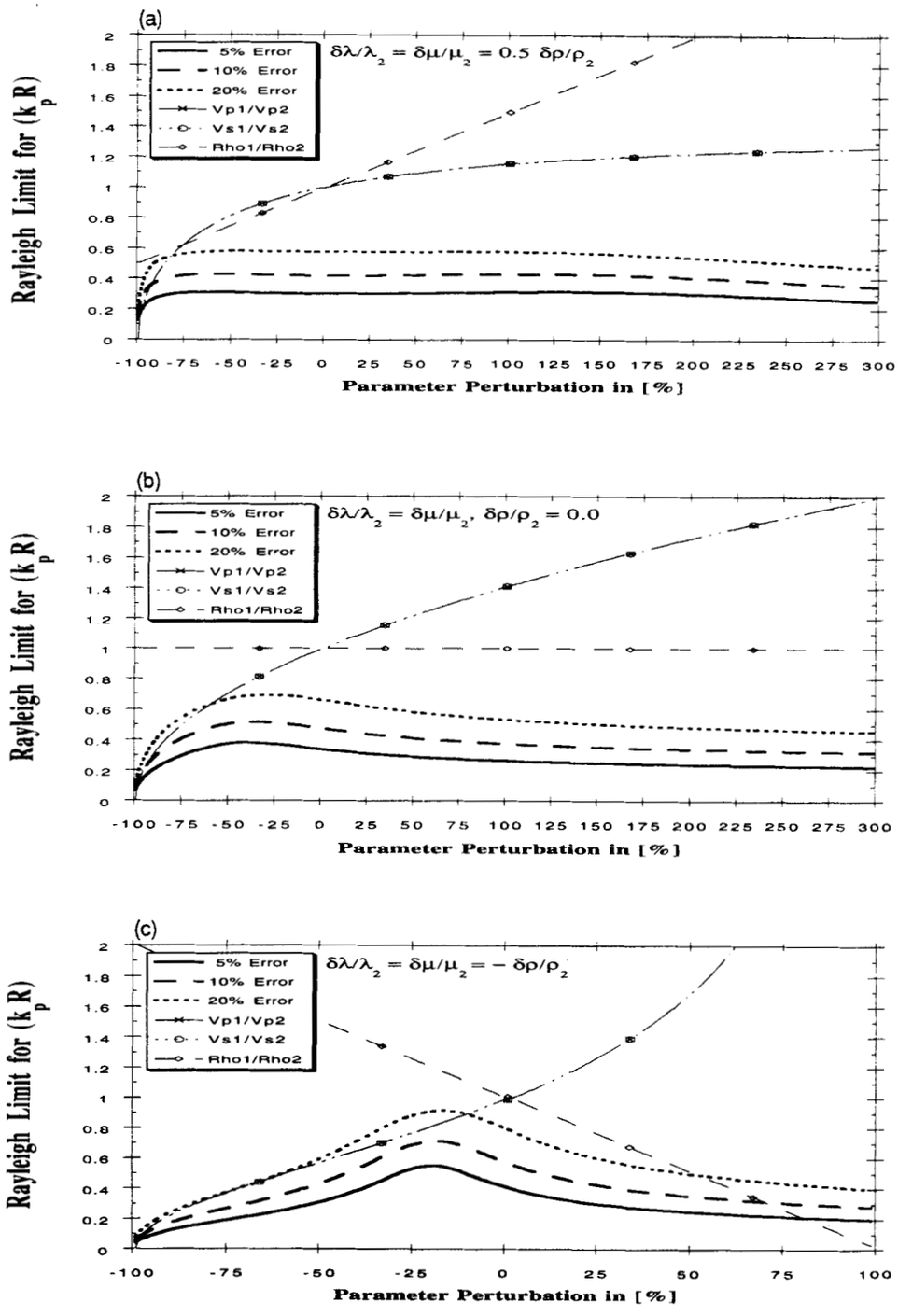

Figure 7. Rayleigh limit for the parameter k_pR as a function of parameter perturbation. The three curves correspond to three investigated error limits of 5 per cent, 10 per cent and 20 per cent. Also plotted are the velocity and density ratios associated with the chosen relation between the elastic parameters.

density were selected. In addition, the velocity and density ratios are indicated to demonstrate the effect of the parameter perturbations. In the presented examples, we keep the sign and increase in perturbation equal for λ and μ, while the associated change in ρ varies in sign and magnitude. Fig. 7(a) denotes the situation of a 50 per cent reduced density increase in relation to the other parameters. The curves for the Rayleigh limit show a parallel trend for the different errors, with a smooth flat level between −75 per cent and +100 per cent. For higher perturbations a slow decrease in the Rayleigh limit is observable. However, towards −100 per cent the limit drops steeply, indicating a small value for the Rayleigh limit of a very low-velocity inclusion. This result has a natural explanation in the fact that $k_\rho R$ inside the inclusion becomes large and violates the Rayleigh limit condition. Changing the relation between the parameter perturbations will affect the shape of the curves as seen in the next examples. In Fig. 7(b), we kept the density at a constant level that produced a maximum in the Rayleigh limit for perturbations between −25 per cent and −50 per cent. This maximum is caused by the mutual influence of an underestimation of the behaviour of the Rayleigh solution for low-velocity obstacles in the Mie diffraction region ($k_\rho R \approx 1$) and a general overestimation of the trend of the solution at high frequencies. At some point these two processes compensate each other. Numerical examples illustrating this phenomenon and a discussion may be found in Korneev & Johnson (1993b). For a third relation between the elastic parameters (Fig. 7c), the maximum is reached for a lower negative perturbation with a different amplitude. In both cases the trend of the curves for positive perturbations remains the same, indicating a continuously increasing deviation between the Rayleigh approximation and the exact solution.

The results clearly suggest that the Rayleigh limit has a more flexible interpretation than indicated by condition (29). Depending on the acceptable error between the Rayleigh approximation and the exact solution, we find values for the Rayleigh limit between 0.3 and 0.8 for a positive increase in parameter perturbation, and limits of up to 0.9 for negative perturbations. The constant shift between the graphs for the three errors over the entire range of perturbation indicates a relation between the error and the Rayleigh limit $(k_\rho R)_{\text{lim}}$ which can be found from the equation

$$\Delta e = d(k_\rho R)^2_{\text{lim}}, \tag{30}$$

where Δe is the allowed error, and d a constant, defined by the perturbation in the elastic parameters from the background. In order to approximate the magnitude of d, we go back to the exact solution for the sphere (eq. 3), and derive a low-frequency approximation based on frequency terms up to fifth order (ω^5), thus using the first four coefficients ($l = 0, 1, 2, 3$) of the exact solution. By comparing the parameter $k_\rho R$ of this improved approximation, and the Rayleigh approximation based on third-order terms (eq. 6), we are able to evaluate d. Using the notation and assumptions from eq. (27) we get in the vicinity of zero perturbation

$$d \approx 0.4\left(\frac{7n^2 + 5n + 2}{6.4n^2 + 1.6}\right)^{1/2}.$$

Thus, for the low-frequency Rayleigh approximation (eq. 6), eq. (30) provides a means to estimate the error of the Rayleigh limit with a minimum knowledge of the parameters involved.

6 CONCLUSIONS

The intention of this paper was to investigate the accuracy of several asymptotic solutions to the problem of low-frequency elastic-wave scattering and to provide means to evaluate scattering experiments in their planning stage. The results were kept in universal format, allowing for a convenient application to various scattering problems in seismology, varying from local over crustal-to-mantle scale lengths.

We investigated a low-frequency total-field solution to the problem of elastic Rayleigh scattering, which produced, within the Rayleigh limits, exact results over the entire distance range of observation, and compared it to pure near- and far-field solutions. The generally used far-field solution cannot be applied to the case of an inhomogeneity situated within a distance less than two wavelengths from the point of observation. Within this distance, the near-field terms dominate the amplitude of the scattered wave, and P and S waves cannot be separated. This case, dependent on the wavelength of the incident wave, may arise in cross-hole experiments when the inhomogeneity is located close to the observation well and in experiments where the scattering object is sited in the uppermost crust beneath the detecting system. The inversion for the perturbation in the elastic parameters will fail if a Green function is applied that does not contain the appropriate near-field terms. However, at a distance farther than 2λ, the near-field terms have decayed sufficiently and the far-field solution can be applied. At this distance, the mean value of the relative error between total- and far-field solutions is 15 per cent and 2 per cent for the $\hat{\mathbf{r}}$ and $\hat{\boldsymbol{\theta}}$ components, respectively. The generalized amplitude–distance relations (Figs 2, 3) can be used to determine the scattered amplitudes for any case of low-frequency elastic-wave scattering as long as the results are normalized by the actual experiment parameter $k_\rho R$.

The availability of an exact solution enabled us to compute errors for the application of the Rayleigh approximation and associated solutions and investigate them as a function of various parameters. The representation of the non-linear Rayleigh approximation as a linear and quadratic Rayleigh–Born approximation revealed, for the relative error, a strong dependence on the scattering angle for both the $\hat{\mathbf{r}}$ and $\hat{\boldsymbol{\theta}}$ components. For a fixed-parameter perturbation, it was found that the $\hat{\mathbf{r}}$ component

incurs a larger error for forward scattering than for scattering perpendicular to the direction of incidence. Four distinct lobes about 45° off the axis of wave incidence developed for the error in the $\hat{\boldsymbol{\theta}}$ component. In both cases the application of the quadratic Rayleigh–Born approximation reduced this error by a factor of 5. These results suggest that if the orientation of primary source, scatterer and receiver are known, then it is possible to estimate the accuracy of the approximation due to linearization of the problem.

The increase in magnitude of parameter perturbation caused increasing magnitudes in the relative error for linear and quadratic approximations, although the exact amount depends on the sign of the perturbation. For a positive increase of 100 per cent, the maximum error amounts to 9 per cent and 17 per cent for the quadratic and linear Rayleigh–Born approximations, respectively. A decrease in elastic parameters caused a larger error. For the case of a void (−100 per cent), the deviation was determined to be 19 per cent for the quadratic and 37 per cent for the linear approximation. As a consequence, a more flexible interpretation of the magnitude of parameter perturbation is justified. As could be seen, the inequality (eq. 18) represents a very conservative limit, whereas a linearization in the case of perturbations below ~20 per cent should produce reliable results. In the case of inversion for the parameter perturbations, the difference between the linear and quadratic Rayleigh–Born approximations can be applied to correct the result after every iteration in the inversion procedure. A faster and more stable algorithm should be the result.

In order to facilitate the estimation of the relative error due to linearization of the problem, we derived an approximation of the error, entirely based on the deviations in the elastic parameters from the background. This enables one to estimate the error prior to an experiment based on a minimum of information and may help to improve the planning of the investigations. We found our equation to provide an adequate representation of the relative error in the linear Rayleigh–Born approximation for a parameter perturbation of up to ±20 per cent.

One of the assumptions of the Rayleigh approximation is that the value of $k_p R$ is small compared to 1. However, thus far no exact evaluation of this limit has been performed. We investigated the Rayleigh limit for $k_p R$ as a function of perturbation in the elastic parameters. Allowing for various errors between the exact solution and Rayleigh approximation, we found surprisingly high values for the limit over almost the entire range of perturbation between −100 per cent and +300 per cent. Maximum values of more than 0.9 were reached. A relation between the Rayleigh limit and the accepted error as a function of parameter perturbation was found. The high values for the Rayleigh limit allow the validity of Rayleigh scattering (eq. 29) to be extended further toward the range of Mie scattering ($R \rightarrow \lambda$), and thus open a broader range for the application of elastic-wave Rayleigh scattering.

ACKNOWLEDGMENTS

Data processing was carried out at the Center for Computational Seismology, Lawrence Berkeley Laboratory, under support from the Director, Office of Energy Research, Office of Basic Energy Sciences, Geosciences Program, through U.S. Department of Energy contract DE-AC03-76F00098. Support was also provided by grant EAR-9105515 of the National Science Foundation. One of the authors (R.G.) gratefully acknowledges the financial support of the German Academic Exchange Service (DAAD).

REFERENCES

Aki, K., 1969. Analysis of the seismic coda of local earthquakes as scattered waves, *J. geophys. Res.*, **74,** 615–631.

Aki, K., 1980. Attenuation of shear waves in the lithosphere for frequencies from 0.05 to 25 Hz, *Phys. Earth planet. Inter.*, **21,** 50–60.

Doornbos, D.J., 1976. Characteristics of lower mantle inhomogeneities from scattered waves, *Geophys. J. R. astr. Soc.*, **44,** 447–470.

Frankel, A., 1991. Mechanisms of seismic attenuation in the crust: scattering and anelasticity in New York State, South Africa, and Southern California, *J. geophys. Res.*, **96,** 6269–6289.

Frankel, A. & Clayton, R.W., 1986. Finite difference simulations of seismic scattering: Implications for the propagation of short-period seismic waves in the crust and models of crustal heterogeneity, *J. geophys. Res.*, **91,** 6465–6489.

Frankel, A. & Wennerberg, L., 1987. Energy-flux model of seismic coda: separation of scattering and intrinsic attenuation, *Bull. seism. Soc. Am.*, **77,** 1223–1251.

Haddon, R.A.W. & Cleary, J.R., 1974. Evidence for scattering of seismic *PKP* waves near the mantle–core boundary, *Phys. Earth planet. Inter.*, **8,** 211–234.

Herraiz, M. & Espinosa, A.F., 1987. Coda Waves: A Review, *PAGEOPH*, **25,** 499–577.

Hudson, J.A. & Heritage, J.R., 1981. The use of the Born approximation in the seismic scattering problem, *Geophys. J. R. astr. Soc.*, **66,** 221–240.

Korneev, V.A. & Johnson, L.R., 1993a. Scattering of elastic waves by a spherical inclusion—1. Theory and numerical results, *Geophys. J. Int.*, **115,** 230–250.

Korneev, V.A. & Johnson, L.R., 1993b. Scattering of elastic waves by a spherical inclusion—2. Limitation of asymptotic solutions, *Geophys. J. Int.*, **115,** 251–263.

O'Doherty, R.F. & Anstey, N.A., 1971. Reflections on Amplitudes, *Geophys. Prospect.*, **19,** 430–458.

Richards, P.G. & Menke, W., 1983. The apparent attenuation of a scattering medium, *Bull. seism. Soc. Am.*, **73,** 1005–1021.

Sams, M. & Goldberg, D., 1990. The validity of Q estimates from borehole data using spectral ratios, *Geophysics*, **55,** 97–101.

Sato, H., 1984. Attenuation and envelope formation of the three-component seismograms of small local earthquakes in randomly inhomogeneous lithosphere, *J. geophys. Res.*, **89**, 1221–1241.

Shapiro, S.A. & Zien H., 1993. The O'Doherty–Anstey formula and localization of seismic waves, *Geophysics*, **58**, 736–740.

Tarantola, A., 1986. A strategy for nonlinear elastic inversion of seismic reflection data, *Geophysics*, **51**, 1893–1903.

White, B., Sheng, P. & Nair, B., 1990. Localization and backscattering spectrum of seismic waves in stratified lithology, *Geophysics*, **55**, 1158–1165.

White, B., Sheng P., Zang Z.Q. & Papanicolaou G., 1987. Wave localization characteristics in the time domain, *Phys. Rev. Lett.*, **63**, 1918–1921.

Wu, R.S., 1982. Attenuation of short period seismic waves due to scattering, *Geophys Res. Lett.*, **9**, 9–12.

Wu, R. & Aki, K., 1985. Scattering characteristics of elastic waves by an elastic heterogeneity, *Geophysics*, **50**, 582–595.